Study of Computational Issues in Simulation of Transient Flow in Continuous Casting

Quan Yuan, Bin Zhao, Pratap Vanka, Brian G. Thomas

Department of Mechanical and Industrial Engineering, University of Illinois, Urbana, IL, USA

Unsteady three-dimensional turbulent flow and heat transport in the liquid pool during continuous casting of steel slabs has been computed using several different computational models, domains, grids, and inlet conditions. The most advanced computations employ a large-eddy simulation code, UIFLOW with a second-order central-differencing scheme, 1.6 million nodes and a realistic simulation domain including the complete submerged entry nozzle. The model has been validated in previous work through comparison with PIV measurements in caster water models, and with velocity and temperature measurements in an operating steel caster. The present computations are compared with flow measurements in a full-scale water model and with heat flux measurements in a jet impingement test problem. Results are compared between model domains of the full caster with symmetric half-caster and two-fold symmetric quarter-caster simulations. The effects of thermal buoyancy and the solidifying steel shell walls are studied independently. The effect of different inlet conditions is investigated by comparing results including nozzle simulations that are both coupled and uncoupled with the mold domain and a simplified nozzle geometry. The importance of the Sub-grid scale (SGS) model for treating the small turbulent eddies is investigated through simulations with and without the Horiuti SGS K model. A rigorous grid refinement study is undertaken, which indicates criteria for choosing the element size near the walls. Accurate heat transfer predictions are more difficult to attain than accurate velocities. Finally, comparisons are made with Reynolds-averaged approaches, including standard K-ε and low Re-number K-ε model computations of the same system. The relative advantages and disadvantages of the different flow simulation methods are evaluated.

Keywords: Turbulent fluid flow, continuous casting, submerged entry nozzles, slab molds, superheat removal, computational modeling, large eddy simulation, SGS models, K-ε model, PIV, mesh refinement, symmetry, jet impingement.

Introduction

Computational fluid dynamics (CFD) is becoming a powerful tool to study turbulent fluid flow in complex metallurgical processes, such as the continuous casting of steel slabs. These fundamentally-based mathematical models have advantages over other tools, such as water models and plant experiments, owing to their ability to quickly and accurately visualize and quantify flow patterns and related phenomena such as free surface motion, multiphase particle transport and entrapment, and heat transfer. Furthermore, their use is rapidly accelerating, due to the tremendous increases in computer hardware and software, which doubles in power about every 1.5 years [1].

Although CFD models are growing in power and complexity, accurate results are often difficult to achieve. This can be due to modeling assumptions in the turbulence model, inappropriate assumption of flow symmetry, insufficient domain size, oversimplified inlet conditions, inadequate mesh refinement, convergence problems, poor choice of boundary conditions such as wall laws and outlet conditions, and many others. Many different modelling choices are available, and the best choice is often problem dependent. Thus, the present work was undertaken to investigate some of the issues affecting the numerical accuracy of CFD models in the context of turbulent flow in the nozzle and mold during the continuous casting of steel slabs. Based on the results of many simulations of the same system with different models, guidelines are offered for choosing the simulation domain, symmetry assumption, inlet conditions, mesh refinement, and turbulence model. This work should be useful for developing future models of continuous casting, or similar flow systems, and in evaluating the accuracy of the results.

Previous Work

In spite of the widespread application of CFD models to continuous casting, and the many different modeling options that are available, relatively few studies have systematically investigated the numerical accuracy of CFD models of this system. The accuracy of CFD models has been investigated systematically in other systems [2-4]. Najjar et al. [5, 6] studied the effects of inlet conditions and wall laws on velocity distribution in a continuous slab casting mold fed from a bifurcated nozzle using a 2-D finite-element K-ε model. They developed guidelines for achieving efficient convergence, consisting of larger relaxation factors for early iterations to accelerate reduction of the initial error, followed by smaller relaxation factors to maintain stable convergence. A new wall law was found to produce better accuracy than the standard wall law for this flow problem involving jet impingement and recirculation. Inlet conditions, including those for turbulence parameters, had a huge influence on the flow pattern. Hershey et al. [7] found that uncoupling the nozzle and mold simulations was reasonable, as it produced only small differences in the flow pattern near the recirculation region near the upper ports.

Thomas et al. [8] compared 4 different methods for studying fluid flow in slab casting. Two different modelling approaches both matched well with measurements in a water model and in an actual steel caster. The standard K-ε model was able to simulate the time averaged 3-D flow pattern with almost equal accuracy to a fully-transient, large eddy

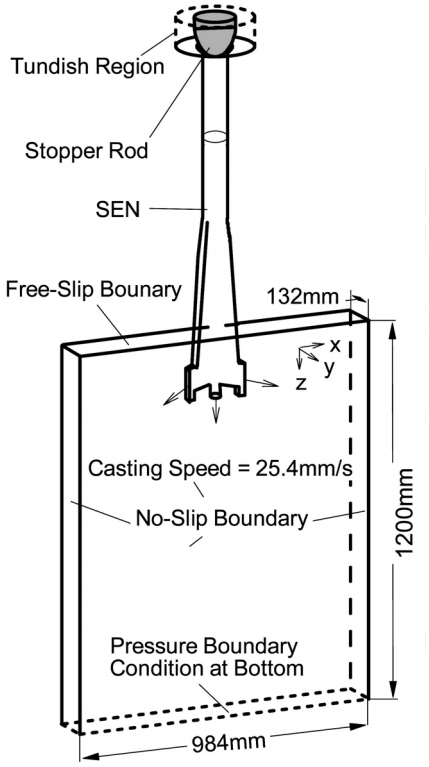

Figure 1. Schematic of the nozzle and mold domains [10].

Table 1. Parameters and properties for steel caster simulation.

Mold (domain) thickness	132	mm
Mold width	984	mm
Model domain width	492	mm
Nozzle domain length (to port top)	687	mm
Strand domain length	1.2	m
Model domain length (total)	1.76	m
Nozzle bore diameter	70	mm
Side Nozzle port height	75	mm
Side Nozzle port width	32	mm
Bottom Nozzle port diameter	32	mm
SEN submergence depth	127	mm
Casting speed	25.4	$mm \cdot s^{-1}$
Casting temperature	1832	K
Steel composition	Low Carbon	
Steel liquidus temperature	1775	K
Reference temperature, T_0	1775	K
Laminar viscosity	0.00555	$kg \cdot m^{-1} \cdot s^{-1}$
Thermal conductivity	26	$W \cdot m^{-1} \cdot K^{-1}$
Density	7020	$kg \cdot m^{-3}$
Specific heat	680	$J \cdot kg^{-1} \cdot K^{-1}$
Thermal expansion coefficient	1.0×10^{-4}	K^{-1}
Gravity acceleration	9.8	$m \cdot s^{-2}$
Reynolds number (at side ports)	2.8×10^5	

simulation with a fine mesh, as compared with Particle Image Velocimetry measurements and measurements in an operating steel slab casting mold. However, the K-ε model was less accurate for time-related phenomena, such as the turbulent kinetic energy distribution and flow oscillations. These and other related phenomena, such as the distribution of superheat, the transport and removal of inclusion particles, and the multiphase interactions between the top surface of the steel and the flux layers above are much more important than the fluid flow itself. The accuracy of CFD predictions of these phenomena has not been compared quantitatively.

This work focuses on single-phase fluid flow and heat transfer in a continuous caster of stainless thin slabs [9] pictured in **figure 1** for the conditions given in **table 1**. Previous work [10, 11] has demonstrated that predictions of an LES model of transient flow in this caster matches well with measurements in a water model, including the flow velocities, [10] top surface contour, and particle flotation rates [11]. The present work investigates computational issues involved in obtaining accurate predictions of this system, including the time averaged flow pattern, transient behaviour, and heat transfer in the molten pool.

Flow Model Equations

The models in this work solve the three-dimensional Navier-Stokes equations which govern the conservation of mass and fluid momentum:

$$\frac{\partial v_i}{\partial x_i} = 0 \tag{1}$$

$$\rho\left(\frac{\partial}{\partial t}v_i + \frac{\partial}{\partial x_j}v_j v_i\right) = -\frac{\partial P}{\partial x_i} + \frac{\partial}{\partial x_j}\mu_{eff}\left(\frac{\partial v_j}{\partial x_i} + \frac{\partial v_i}{\partial x_j}\right) \tag{2}$$

$$\text{where: } \mu_{eff} = \mu_0 + \mu_t \tag{3}$$

In the large eddy simulations (LES), the time-dependent unknown velocities, v_i, represent the large scale eddies, as the effect of the small scale eddies is approximated with a sub-grid scale (SGS) model. In some simulations, the turbulent viscosity, μ_t, is set to zero, which can be interpreted as coarse-grid DNS (direct numerical simulations). Numerical diffusion from the discretization scheme and coarse grid can be interpreted as creating some artificial turbulent viscosity in these simulations.

In the SGS-K model [12], turbulent viscosity is approximated by:

$$\mu_t = 0.05\rho K_G^{1/2}\Delta \tag{4}$$

$$\text{where } \Delta = (\Delta_x \Delta_y \Delta_z)^{1/3} \tag{5}$$

and Δ_i is the grid spacing in the x, y, or z direction. The SGS kinetic energy K_G is found by solving the following extra transport equation:

$$\rho\left(\frac{\partial K_G}{\partial t}+v_j\frac{\partial K_G}{\partial x_j}\right)=\frac{1}{2}\mu_t\left(\frac{\partial v_i}{\partial x_j}\frac{\partial v_i}{\partial x_j}+\frac{\partial v_i}{\partial x_j}\frac{\partial v_j}{\partial x_i}\right)$$
$$-\rho\frac{K_G^{3/2}}{\Delta}+\frac{\partial}{\partial x_i}\left[(\mu_0+0.1\rho K_G^{1/2}\Delta)\frac{\partial K_G}{\partial x_i}\right] \quad (6)$$

In the standard K-ε model simulations, only the time-averaged velocity field is solved and the turbulent viscosity is defined by:

$$\mu_t=c_\mu\rho\frac{K^2}{\varepsilon} \quad (7)$$

where $c_\mu = 0.09$. This approach requires solving two additional partial differential equations for the transport of turbulent kinetic energy, K (m^2/s^2), and its dissipation, ε (m^2/s^3).

In the low-Re K-ε model, the turbulence is gradually diminished towards laminar flow in the low velocity regions such as near the walls, by redefining c_μ as a function of the local turbulent Reynold's number, Re_T,

$$c_\mu=0.09\exp\left(\frac{-3.4}{(1+\mathrm{Re}_T/50)^2}\right) \quad (8)$$

$$\text{where } \mathrm{Re}_T=\frac{\rho K^2}{\mu\varepsilon} \quad (9)$$

In addition, extra terms appear in the K and ε transport equations, as defined elsewhere [13, 14].

Boundary Conditions

Inlet. The liquid pool is fed by a trifurcated nozzle, which has an important influence on the flow pattern. [8] Thus nozzle simulations were conducted to acquire accurate inlet conditions to the mold. For uncoupled simulations, unsteady flow velocities leaving the nozzle ports were collected at regular time intervals and recycled periodically as the inlet conditions for the liquid pool simulations. As shown in figure 1, the 1.1-m long nozzle extends from the tundish bottom and is fed through the annulus formed by a 64.4% open stopper rod, down a 70-mm diameter round bore upper nozzle that tapered into a thin trifurcated outlet region. The flow pattern computed in the complete nozzle is shown in **figure 2**, showing close-ups near the stopper rod, and the nozzle exit ports. Simplified simulations of just half of the nozzle were also performed, starting from a uniform velocity profile 293mm below the stopper rod. Some simulations with this nozzle were also coupled with the mold domain in the same grid.

Outlet. For simulation efficiency, the computational domain of the water model simulated in this work is obtained by truncating the 2.6m long physical domain at a plane 1.2m below the top surface. This generates an artificial outlet plane. A simulation is also performed of the real thin-slab caster, which differs by gradually tapering the liquid pool that is contained within the solidifying shell, and truncating it at 2.4m below the top surface. A constant pressure boundary condition, with zero gradient of other variables, was used at the outlet planes where the flow becomes nearly uniform.

Top Surface and Symmetry Plane(s). The effect of assuming symmetry is investigated by comparing full pool, half pool, and quarter pool simulations. A free-slip condition was imposed at symmetry plane(s) to represent center plane(s). Specifically, the normal velocity and the normal gradients of pressure and the other two velocity components were set to zero. The same condition was imposed on the top surface. The predictions of this work (presented later) match previous measurements [10] that the top surface is relatively quiescent, so a model for free surface deformation is not necessary to accurately model the flow.

Narrow Face and Wide Face Walls. Water models and steel casters have very different walls. Water models have stationary straight plastic side walls representing the solidification front. Thus all three velocity components were set to zero at the wall boundaries. Flow in the steel caster was modeled up to, but not including, the front of the downward moving mushy zone [15], where solidification occurs to take away mass from the molten steel pool. In addition to

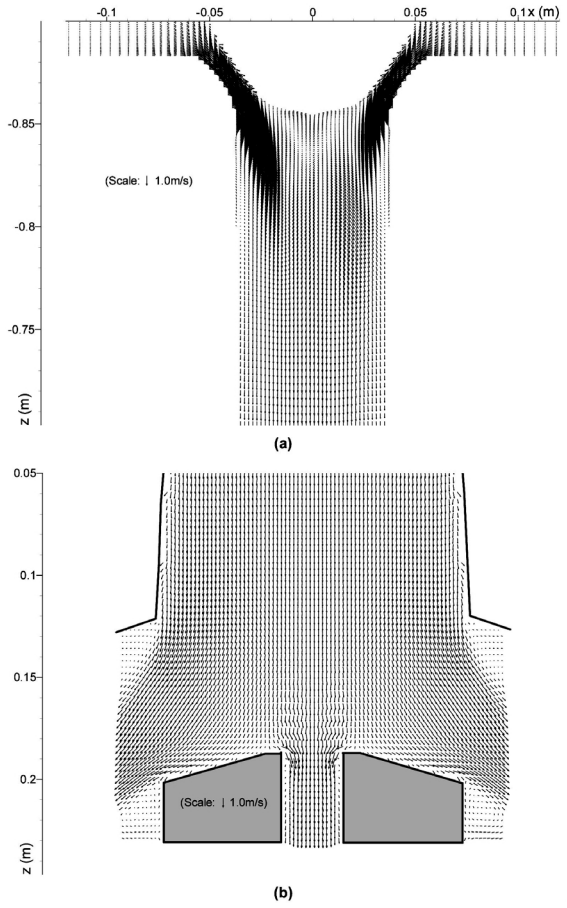

Figure 2. Computed flow velocities in nozzle near (a) stopper rod and (b) exit ports.

tapering the domain walls, the mass transfer across the solidification front was modelled with the following velocity boundary conditions [10]:

$$v_x = \left(\frac{\rho_s}{\rho_l} - 1\right) \sin\theta \cos\theta V_{casting} \quad (10a)$$

$$v_z = \left(\frac{\rho_s}{\rho_l} \sin^2\theta + \cos^2\theta\right) V_{casting} \quad (10b)$$

where ρ_s and ρ_l are the solid and liquid densities, the casting speed is $V_{casting}$, and the solidification front makes an angle θ with the casting direction that decreases with distance below the meniscus.

In the standard K-ε model simulations, standard wall functions were used to represent the high gradients of velocity, kinetic energy, and dissipation near the walls [13]. The normal distance from the wall to the first node, n, is expressed in non-dimensional form, y^+, defined as

$$y^+ = \frac{\rho C_\mu^{0.25} K^{0.5}}{\mu} n \quad (11)$$

The tangential velocity profile V_t as a function of y^+ is

$$V_t = \begin{cases} -(C_\mu K)^{0.5} y^+, & for\ y^+ < y_o^+ \\ \dfrac{-(C_\mu K)^{0.5}}{\kappa} \log(E y^+), & for\ y^+ \geq y_0^+ \end{cases} \quad (12)$$

where E=9.0 is the roughness constant, κ=0.41 is the Von-Karman constant and y_0^+ is the cross over point between the viscous sub-layer and the logarithmic region.

The wall law for the K equation (K-ε model) is simply a zero gradient condition at the wall. Turbulence dissipation at the wall is calculated from K using the relation: [13]

$$\varepsilon_{(y^+=0)} = \frac{C_\mu^{0.75} K^{1.5}}{\kappa n} \quad (13)$$

The LES and low Re K-ε models do not use wall functions, and simply set the velocity components and turbulence parameters K and ε to zero at the walls.

Solution Procedure

In the LES computations, the time-dependent three-dimensional Navier-Stokes equations are discretized using the Harlow-Welch fractional step procedure [16]. Second-order central differencing is used for the convection terms and the Crank-Nicolson scheme [17] is used for the diffusion terms. The Adams-Bashforth scheme [18] is used to discretize in time with second order accuracy. The pressure Poisson equation is solved using an algebraic multi-grid (AMG) solver [19] on an unstructured Cartesian grid.

Computational Details

The computational domain is presented in figure 1. The geometry, casting conditions, material properties and computational parameters are given in table 1. There is no argon gas in any of the simulations in order to match the real caster, where calcium treatment was used to avoid nozzle clogging. The LES computations employed the in-house CFD code, UIFLOW [20]. The K-ε model results [14] were computed with the commercial package CFX [13].

For computational efficiency, the domain was divided into nozzle and liquid pool regions for most simulations. A full nozzle LES simulation with a 0.6 million cell mesh took 10 days on a Pentium IV 1.7GHz CPU for a 9.45s simulation. Transient velocities exiting the trifurcated nozzle ports were stored every 0.025s and used as inflow conditions to the liquid pool. An LES simulation of the full mold region (no symmetry assumption) with 1.3 million cells took 29.5 CPU-s per time step or 24 days for 70,000 time steps (70s of real time). Most K-ε models employed a 0.3 million node grid and required only a few hours to run. Further computational details are given elsewhere [10, 11, 14, 21].

Flow Velocity Results

Before a computational model is applied to investigate the problem of interest, it should first be validated by comparison with a known solution, to verify that the computational method is accurate, and that the grid is sufficiently refined. It should then be compared with measurements of a similar system, to validate that the modelling approach, domain, boundary conditions, and properties are all reasonable.

The codes used in this work were first run to match analytical solutions of simple test problems such as flow in round and square pipes [20]. The next step of numerical validation is to demonstrate "grid independence", by comparing the results of simulations on successively finer computational meshes for the specific problem of interest.

Effect of Grid Resolution

To investigate the effect of mesh refinement, LES computations were performed on six different grids, containing 0.02, 0.08, 0.10, 0.20, 0.40, and 0.80 million cells. Assuming symmetry between the right and left sides, the computational domain was one half of the physical domain. All simulations were performed with the SGS K-model and ignored buoyancy effects. The inlet conditions for these simulations were taken from a 100s half-nozzle simulation corresponding with the finest grid, stored every 0.001s.

The grids were all stretched with a factor of 1.01-1.03 to produce finer cells near the boundaries where they are most needed for accuracy, owing to the high local changes in gradient. This produced cell-center spacings from the wall at the critical region of jet impingement of 1.5mm, 1.5mm, 2.5mm, 2.5mm, 3mm and 6mm, for the 6 different grids respectively.

Flow patterns in the center plane of three different grids are compared in **figure 3**. The jet traverses across the domain to impinge on the narrow face, where it turns upward to the top surface and back towards the SEN in a classic double roll flow pattern. The two finest grids are almost

identical, showing that grid independence has been achieved. The coarse grid shows an important deviation in jet direction that would have a large adverse effect on secondary calculations, such as particle motion.

To quantify the difference between grids on an equal basis, the velocities computed for each grid were first interpolated onto a 64×128 uniform-spaced grid. Errors for both the time-average and rms velocity were calculated as an average at the center plane y = 0 as follows:

$$Error = \sqrt{\frac{\sum_{i=1}^{N}\left[\left(V_{x,i}-V_{x,j}^{\text{exact}}\right)^2+\left(V_{y,i}-V_{y,i}^{\text{exact}}\right)^2+\left(V_{z,i}-V_{z,i}^{\text{exact}}\right)^2\right]}{N}} \quad (14)$$

where the exact solution was estimated using the results from the finest grid (0.8 million cells).

The time average error results are presented in **figure 4**. This error increases exponentially with increasing grid spacing, which corresponds with decreasing number of cells in the grid. The error between the two finest grids averages only ~0.03m/s, although this represents a 17% difference, relative to the mean velocity in the domain, ~0.18m/s. Coarser grids have errors that are much larger than a glance at the velocity vectors would indicate.

The rms velocity error results are presented in Fig. 4b. This error also increases greatly with coarsening grid size. These results indicate that the mesh resolution prediction of velocity fluctuations is accurate within ~0.02m/s or ~17%. The fluctuating velocity component is almost half of the mean velocity component, indicating that turbulence is very strong. Overall, the fine mesh (0.8 million nodes) is believed to produce reasonable results for engineering purposes.

Validation with Measurements

In addition to numerical validation and demonstration of sufficient mesh refinement, computational models also require comparison with experimental measurements, to ensure that the modelling assumptions are sound. This has been done extensively in previous work [10, 11, 22]. An example is shown in **figure 5**, which compares the velocities computed along the top surface with measurements from videos of die injection into the water model. These particular results are of practical importance because the maximum surface velocity should fall within a critical range (suggested by Kubota to be 0.2-0.4m/s) [23, 24] in order to avoid defects. The measurements are instantaneous, so are expected to fall within the range of velocities computed at this position. The rough agreement suggests that these computational models are able to predict flow in this process.

Effect of Turbulence Model

The results in figure 5 also compare the predictions of different turbulence models. The difference between different models is on the same order as the difference between the models and the measurements. As reported in previous work [8], the K-ε model gives qualitatively the same time-averaged results as the LES models.

This figure also suggests that the effect of adding an SGS-K model [12] is relatively small. Closer analysis of the velocity vector field confirms this, except in regions very close to the nozzle port exits, where the high velocity gradients generate extra turbulent energy, which causes the SGS-K model jet to spread a little more. The general similarity indicates that either the unresolved small turbulent eddies are not very important, or that false diffusion from numerical discretization errors dominates over the sub-grid scale effects.

Effect of Symmetry Assumption

The continuous casting process in figure 1 appears at first glance to contain two-fold symmetry, about the center-

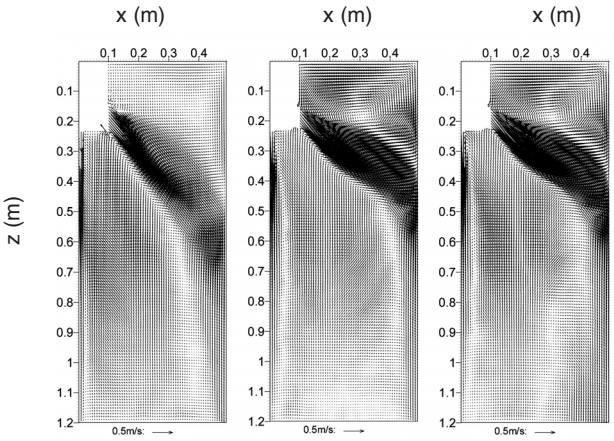

Figure 3. Time-averaged velocity fields at the center plane y=0 obtained from LES with 20x10^3 (left) , 400x10^3 (middle) and 800x10^3 (right) computational cells.

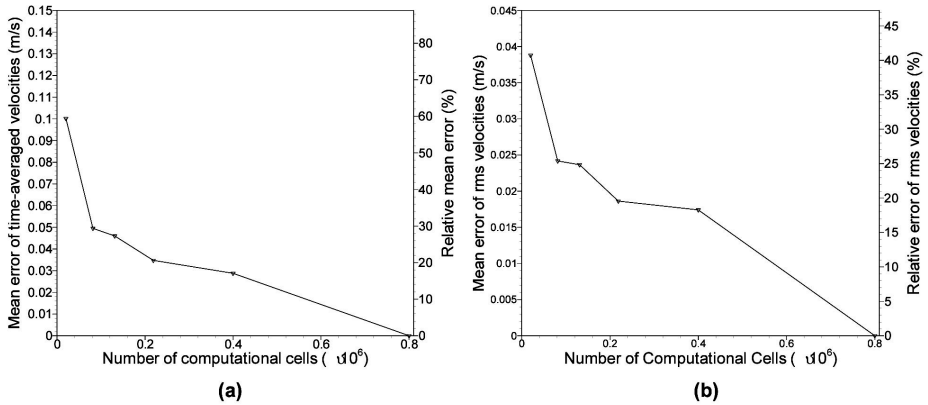

Figure 4. Effect of grid refinement on error in (a) time-averaged and (b) *rms* velocities (acc. to equation (14)).

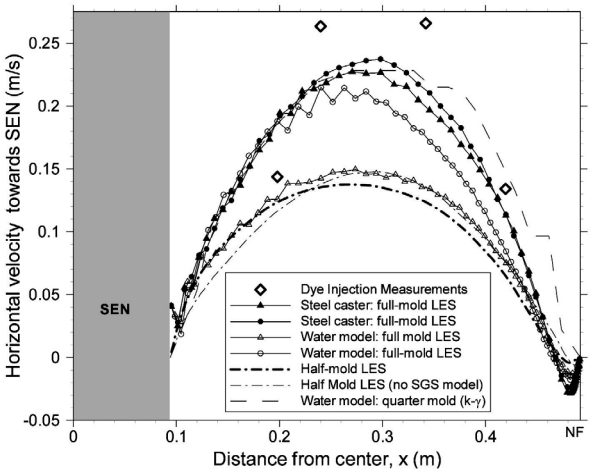

Figure 5. Top surface velocity predictions with different turbulence models.

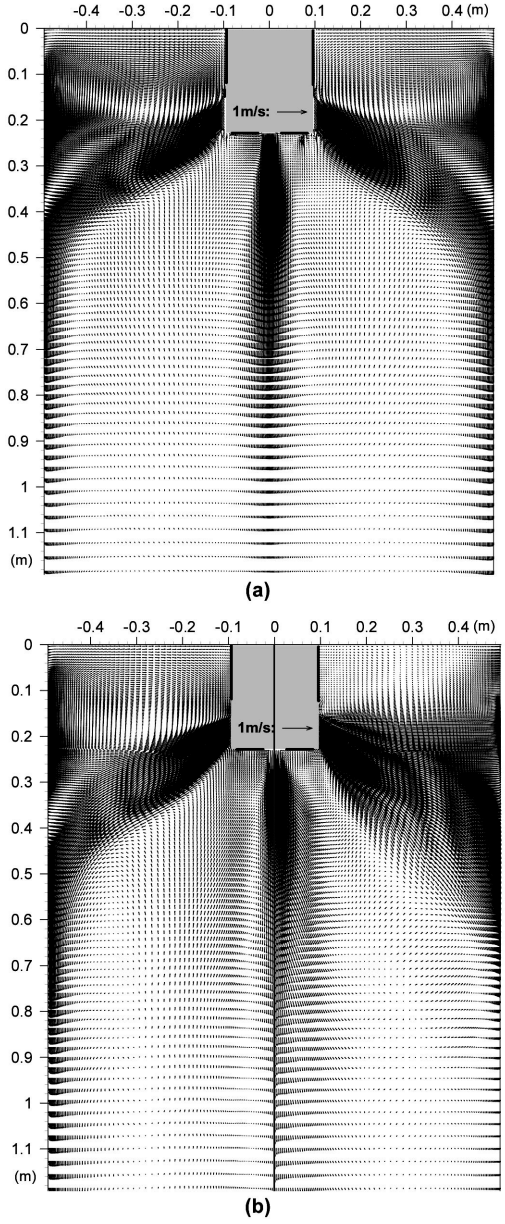

Figure 6. Effect of symmetry assumption on time-averaged velocity fields for simulation domains with (a) both halves (b) half (left) and quarter (right) of the mold region.

planes between the wide and narrow faces. The effect of invoking these symmetry assumptions was investigated by performing simulations on a quarter-domain, half-domain, and a full-domain with no symmetry assumed. The results are compared in **figure 6**.

The full-domain simulation was performed on a 0.74-million cell grid, so has larger cell spacing than the other meshes. However, the differences between the right and left sides of the domain are more significant than the differences between grids. The asymmetries between sides are minor for the time-average flow pattern for this nozzle, but have very detrimental effects on quality in other cases. Large instantaneous variations between sides can only be observed in transient simulations with a full-domain model. Of even greater importance is the exaggerated spreading of the jet in the quarter simulation. This unreasonable result is believed to be caused by the prevention of jet oscillation across the symmetry plane. In the half and full domains, the jet is observed to swirl and oscillate both vertically and horizontally as it traverses the mold. The K-ε model results do not suffer from this problem, as the results in figure 5, were also produced on a quarter domain.

Figure 7 compares the computed speed $(v_x^2 + v_z^2)^{0.5}$ along a vertical line in the caster centerplane, midway between the SEN center and the narrow face. This figure quantifies that the differences between velocity predictions using different model domains are small, except for the poor quarter-domain results.

Figure 8 compares the transient velocity fluctuations predicted using the different domains. The results with the half-domain are similar to the each half of the full-domain model. These rms velocity predictions appear to have roughly equal accuracy as the velocity predictions themselves.

Effect of Inlet Conditions

Previous work has established that inlet conditions have a great effect on the flow pattern [22], so modeling should be extended upstream to simulate flow in the nozzle. The time-averaged velocities in the nozzle were presented in **figure 2** for a 9.5s simulation with the 0.6 million node mesh of the complete nozzle. A slight asymmetry is observed at the top of the nozzle, where flow accelerates past the stopper rod flow control. This does not persist to the lower region of the nozzle, however, as flow disturbances diminish with distance downstream. For this reason, flow entering the mold from a shortened 0.1-million half-nozzle domain (neglecting the stopper rod) was similar. In both cases, most of the flow exits the lower portion of the nozzles, owing to the oversized outlet ports (ratio of total port area to bore area at top of ports is 1.54). The downward angle of the two side jets varies in time from ~30° to 45°. Results from further simplifications of the nozzle were unacceptably different [22].

Uncoupling of the nozzle and mold domains was found in previous work [7] to have negligible adverse effect, which was confirmed in the present work. The combined effects of simplifying the nozzle and coupling the nozzle and mold domains on flow entering the mold is seen in **figure 9** to be

small. The very slight uplifting of flow near the edges of the side ports is believed to be due to the hindrance of flow oscillations inside the nozzle by the half-nozzle domain. The combined effect on flow in the mold of this difference in inlet conditions and the difference between the coarse-grid full mold and fine-grid half-mold simulations is shown in **figure 10** to be small.

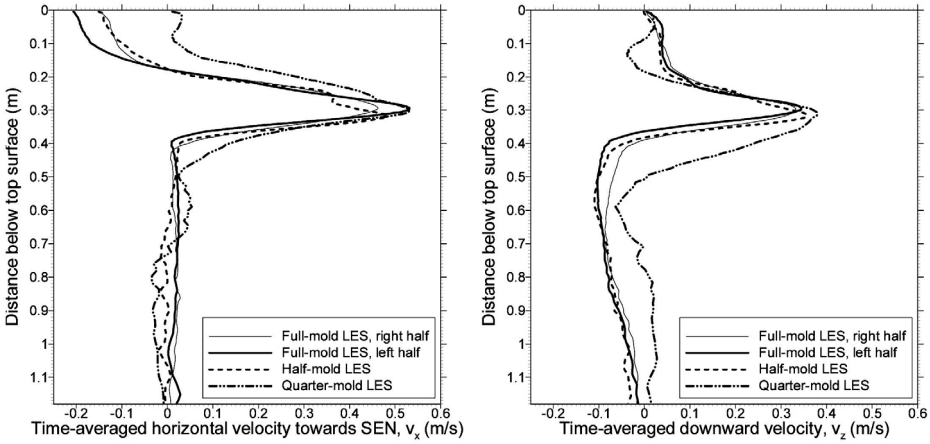

Figure 7. Time-averaged velocities along vertical line 152mm from SEN outlet, from LES.

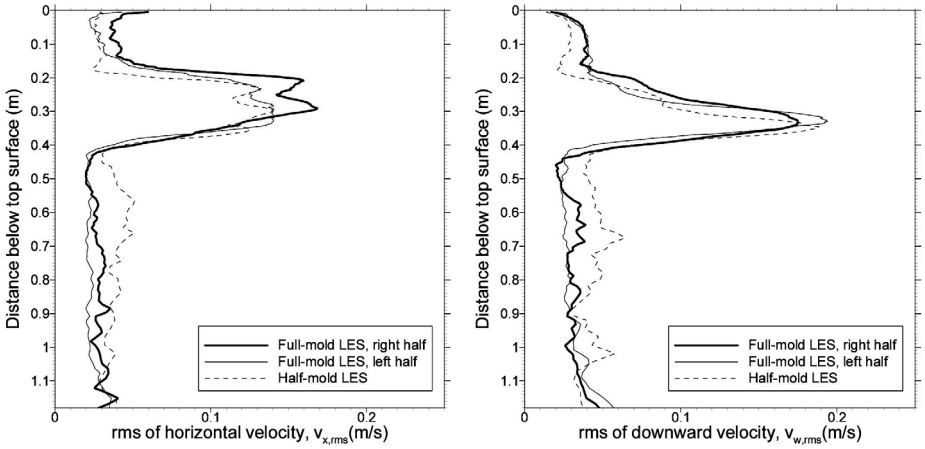

Figure 8. *rms* velocities along vertical line 152mm from SEN outlet, from LES.

Effect of Thermal Buoyancy

A simulation was performed including the effect of natural convection on the flow pattern. To do this, a coupled simulation of superheat transport was performed, as described later. An extra source term was added to the vertical momentum equation, according to the Boussinesq assumption. The simulation domain contained 1.6 million nodes, including the lower 787mm of one half of the nozzle, containing 0.1 million nodes.

The resulting flow pattern is shown in **figure 11**. Compared with the results in figure 3c, there is very little effect of buoyancy. This finding agrees with previous work [25]. A slight upward flow is observed near the top of the nozzle exit, likely due to the slow-moving hotter fluid there relative to the cooler surroundings. Slightly steeper downward flow is observed near the impingement point, perhaps owing to the colder fluid near the wall. The effect of buoyancy appears to be smaller than the other effects studied, so was not investigated further and was neglected in other simulations.

Difference between Water Model and Steel Caster

The combined effects of the solidifying steel shell, and the water model bottom are shown in **figure 12**. The domain of the steel caster has curved side walls, which represent the solidifying front at the liquidus temperature. The boundary shape was obtained from the prediction of an in-house code [26], CON1D, which also agrees with measurements on a breakout shell from this caster [9]. The grid for the 2.4m-long full-domain steel caster contained 1.4 million nodes, with similar mesh spacing to the 0.74 million node grid used for the 1.2m-long water model.

In the top portion of the mold, there is very little difference between the water model and steel caster, as indicated in figure 5. The effect of the moving, porous shell boundary increases with distance below the top surface. **Figure 12** shows that the differences can grow to be quite large by 1m deep. As the shell grows, flow deep within the steel caster tends toward uniform flow much more quickly than flow in the water model. At a given distance, the water model experiences much stronger flows down the narrow face from the side-port jets. It also shows stronger flow down the cen-

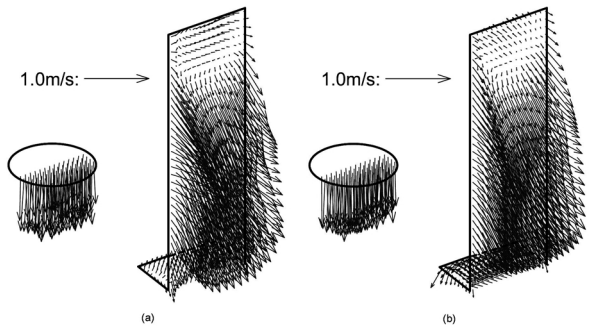

Figure 9. Comparison of time-averaged velocity vectors exiting nozzle ports obtained from (a) coupled simplified nozzle and (b) uncoupled complete nozzle simulations.

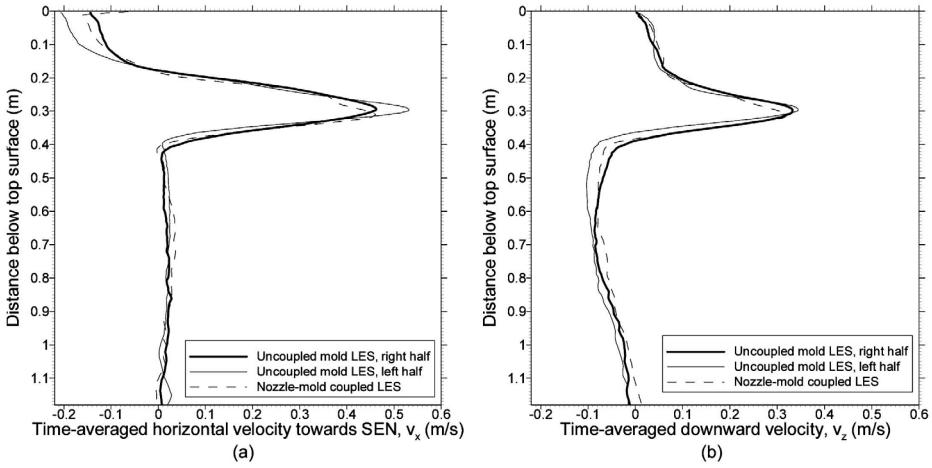

Figure 10. Comparison of time-averaged velocities obtained from nozzle-mold coupled and uncoupled mold simulation along a vertical line 152mm from the SEN outlet plane.

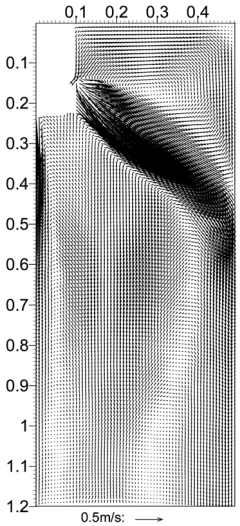

Figure 11. LES half-mold simulation including the effect of thermal buoyancy.

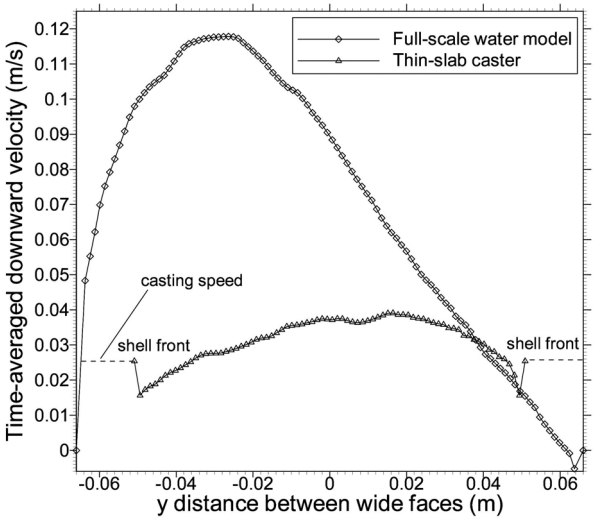

Figure 12. Time-averaged velocities for simulations of water model and steel caster, along a horizontal line 1m below top surface, midway between narrow faces.

ter from the central-port jet of this trifurcated nozzle, as pictured in figure 12. Further details comparing these two systems is given elsewhere [10, 11]. Thus, water models are best applied to investigate surface flow phenomena, such as level fluctuations. Computational models are needed to study internal flows, such as important for particle entrapment and internal segregation.

Superheat Transport Model Description

After simulating the velocity distribution, the transport of superheat was computed by solving the heat conduction equation:

$$\frac{\partial T}{\partial t} + \frac{\partial (u_i T)}{\partial x_i} = \frac{1}{\rho C_p} \frac{\partial}{\partial x_i} \left(k_{eff} \frac{\partial T}{\partial x_i} \right) \qquad (15)$$

$$\text{where } k_{eff} = k + C_p \mu_t / \mathrm{Pr_t} \text{ and } \mathrm{Pr}_t = 0.9 \qquad (16)$$

For the K-ε models, the transient term is neglected. Evaluation of μ_t depends on the turbulence model, as described in the previous section. Fluid is assumed to enter through the inlet fixed at the tundish temperature, as very little heat is lost in the nozzle. The domain walls represent the dendrite tips at the solidification front, so are naturally fixed to the liquidus temperature. The roughness of the dendritic surface and any convection of solidified metal were ignored, owing to the fine columnar structure. For simplicity, the top surface and domain outlet are assumed to be insulated, owing to the small heat flux across these boundaries. Thermal wall laws from Jayatilleke [13, 14, 27] were adopted for the K-ε and low-Re K-ε simulations.

Superheat Transport Results

This section explores the inter-related computational issues of turbulence model, grid resolution, and wall boundary conditions in the modeling of temperature distribution in the liquid pool and heat flux to the solidifying walls. **Figure 13** presents a typical time-averaged temperature field in the nozzle and mold computed by the LES model. The close agreement between the right and left sides confirms that the effect of the subgrid-scale model is negligible.

The velocity and temperature gradients in the vicinity of the laminar sublayer are crucial to the heat flux results. **Figure 14** shows the effect of the turbulence model, wall law, and grid refinement on these gradients. Figure 14a shows profiles of downward velocity at the solidifying shell near the narrowface wall, in the centerplane parallel to the

wide faces, 0.741 mm below the steel – flux interface at the top surface of the domain.

Each point on the graph represents a grid point, so this figure also illustrates the great differences in mesh refinement between the grids. The dashed line for the standard K-ε model illustrates the wall function solution assumed in this model.

This high-speed flow system develops a high velocity gradient near the wall. The LES model (0.74 million nodes) and low-Re K-ε model with the fine grid (0.55 million nodes, y^+<6) and very fine grid (0.84 million nodes, y^+<1) agree in predicting this high velocity gradient. The low-Re K-ε model with the coarse grid (0.3 million nodes, y^+<30) predicts a much lower velocity gradient. Because the LES and low-Re K- ε models do not use wall laws, a fine mesh is needed to resolve velocities in the boundary layer. The unrealistic result illustrates the inaccuracy of using a coarse mesh with the low K- ε model. The wall law in the standard K-ε model is able to capture the steep gradient even with the same coarse mesh (0.3 million nodes).

The heat transfer calculations are more sensitive to the turbulence model and grid size than the flow calculations [28]. Figure 14b shows the corresponding temperature gradients for each turbulence model. Except for the inaccurate coarse-grid low-Re K-ε model, and in the transition region between the laminar sublayer and the bulk, the models roughly agree in temperature predictions both near and far from the wall. The accuracy of the temperature predictions in the bulk has been verified with measurements in this caster, which are reported elsewhere [21, 29, 30].

Figure 15 compares heat flux profiles down the narrow-face centreline predicted using these different turbulence models. The predictions vary widely. The peak heat flux occurs at the jet impingement point. The LES and standard K-ε models have a low heat flux peak at this point, while the user modified K-ε model [14] is slightly higher. The low-Re K-ε models all have extremely high peaks, which become narrower as the grid is refined. The total heat removed along the wall, represented by the area under these curves, is also very large for the y^+<30 and y^+<6 grids. Differences in heat flux predictions are attributed in large part to the wall laws employed by the K-ε models, which generally assume that the first grid point is not in the laminar sublayer.

These results demonstrate the need for sufficient mesh refinement near the laminar boundary region for both the LES and the low-Re K-ε models. Wall laws are tricky to apply with accuracy. Coupled flow-solidification models feature internal solidification fronts that are not known a-priori, so have relatively coarse grids in the boundary layer. The results of this work suggest that these models tend to over-predict heat flux, and consequently produce excessive shell thinning, especially if a low-Re K-ε model is used.

Jet Impingement Test Problem

To further explore accuracy in the prediction of heat flux from jet impingement, a test problem was found where measurements were available for comparison. As illustrated in **figure 16**, this problem consists of an axisymmetric air jet impinging on a cooled flat copper surface. Heat flux to

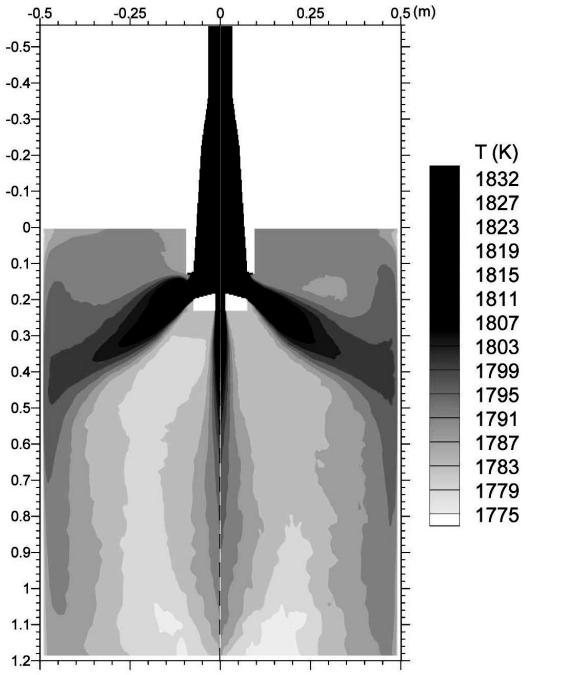

Figure 13. Comparison of temperature field in nozzle and mold region obtained from half-domain simulations with the SGS-K model (left) and no SGS model (right).

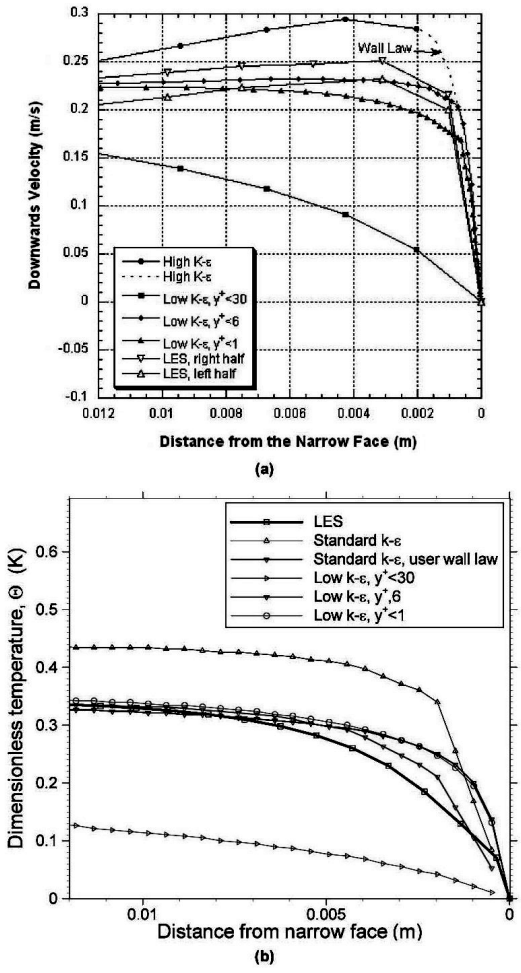

Figure 14. Comparison of different model predictions near narrow-face wall centerline, 0.741m below top surface for a) downward velocity, and b) temperature profile.

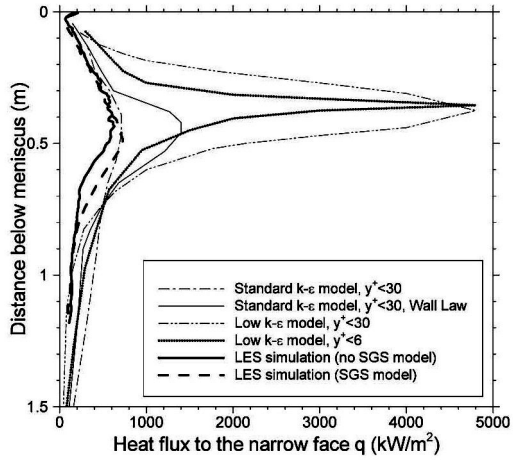

Figure 15. Effect of turbulence model and wall laws on time-averaged heat flux along narrow face center line.

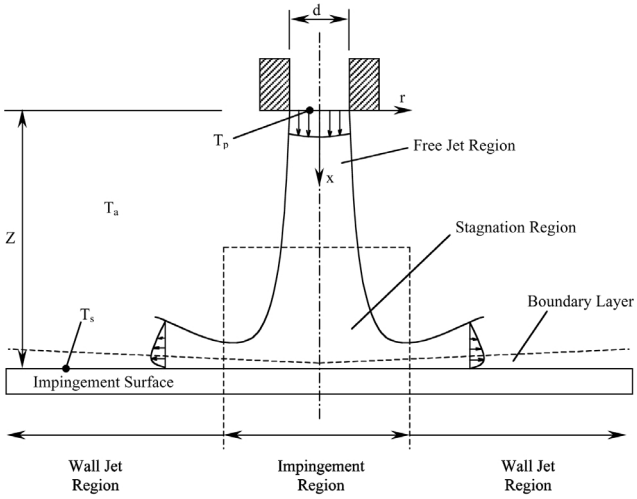

Figure 16. Schematic of impinging jet test problem.

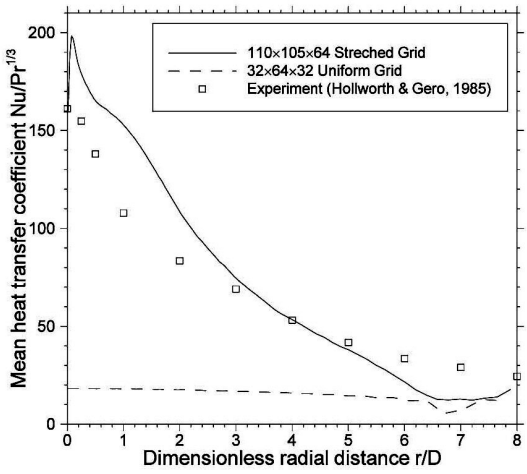

Figure 17. Effect of near-wall grid refinement on test problem heat flux predictions (Re=20000).

the wall was measured as a function of radial distance [31]. Spatial variables are characterized by the inlet nozzle diameter D, given in **table 2**, the nozzle height above the plate, the air properties and temperature conditions. Although the real jet is unconstrained, the 3-D model domain had 160mm diameter, with an exit slit 10mm high. The inlet nozzle domain was assumed to be a ~10D long tube that was perfectly aligned. The velocities are similar to those encountered in the continuous casting process, as characterized by the Re number of 20,000 for this problem.

Figure 17 compares the heat flux predictions along the impingement surface for LES simulations with two different grid spacings with the measurements. Heat flux reaches its maximum near the stagnation point. The impinging jet then turns 90 degrees into a strong radial flow that creates an expanding boundary layer in the wall jet region. Heat flux continually decreases with radial distance.

The cell spacing for the 32x64x32 uniform grid was 0.15625D, where D is the jet inlet diameter. The results greatly under-predict the measurements. This was expected because the maximum heat flux possible with no wall law is limited by the size of the first cell, which was too large.

A simulation was then performed on a 110x105x64 stretched grid (0.8 million cells), where the smallest cell spacing was located near the wall with a value of only 0.006D. This was chosen according to the critical spacing, Δx:

$$\Delta x = k\Delta T/q \tag{17}$$

where ΔT is the temperature difference between the wall and first node and is less than the difference between the inlet and wall temperatures. The heat flux, q, is given in terms of the Nu number:

$$q = Nu(T_{inlet} - T_{wall})k/D \tag{18}$$

The agreement of these results with the measurements appears to validate the accuracy of the LES model, so long as the grid is sufficiently fine.

Table 2. Axisymmetric jet problem conditions.

Inlet diameter D	10	mm
Nozzle to plate distance H	50	mm
Inlet temperature T_{inlet}	25	°C
Ambient temperature Ta	25	°C
Plate surface temperature T_{wall}	8	°C
Density of fluid ρ	1.2	$kg{\cdot}m^{-3}$
Molecular viscosity μ	17.85×10^{-6}	Pa·s
Thermal conductivity k	0.025	$W{\cdot}m^{-1}{\cdot}K^{-1}$
Specific heat Cp	1006	$J{\cdot}kg^{-1}{\cdot}K^{-1}$
Prandtl number Pr	0.71	
Renolds number Re	20000	
Inlet bulk velocity	29.75	$m{\cdot}s^{-1}$
Time step	5×10^{-7}	s

Conclusions

Computational models of turbulent flow have been applied to investigate computational issues in simulation of metallurgical processes. The time-averaged flow pattern is the easiest result to approximate with reasonable accuracy, even with a relatively coarse grid and simplified model. Actual velocity errors are larger than they might appear on a vector plot, however.

Transient phenomena are better modelled with Large Eddy Simulation, but care must taken in choosing the domain and grid. The domain should be extended sufficiently upstream to produce reasonable results in the region of interest. Uncoupling the domains of adjacent regions, such as performing separate calculations of flow in the nozzle and mold, has little effect if the flow between regions does not include much recirculation.

Invoking symmetry by modelling only a quarter of the process is reasonable for time-averaged models, such as K-ε. However, the transient LES models were found to be sensitive to disruption of the real flow oscillations which can produce inaccurate results. For example, a quarter-mold simulation that prevented transverse jet oscillation resulted in exaggerated vertical oscillation, excessive jet spreading, and poor accuracy.

Secondary phenomena such as the prediction of superheat transport are more difficult to model accurately and the results from different models vary widely. Inadequate grid refinement produces very large errors, particularly for the low-Re K-ε model. Further work is needed on turbulence models, wall laws, and grid refinement for heat transfer prediction, especially for processes involving solidification.

Acknowledgements

The authors thank the National Science Foundation (Grant DMI-01-15486) and the member companies of the Continuous Casting Consortium at the University of Illinois at Urbana-Champaign (UIUC) for support which made this research possible. Thanks are also due to former MS student, David Creech, for K-ε computations with CFX that was supplied by AEA Technology, Pittsburgh, and to the National Center for Supercomputing Applications (NCSA) at UIUC for computational facilities.

(A2004074)

Contact: Prof. Brian G. Thomas
Mechanical & Industrial Engineering Dept.
University of Illinois at Urbana-Champaign
1206 West Green Street
Urbana, IL 61801, USA
bgthomas@uiuc.edu (email)

References

[1] Voller, V.R. and Porte-Agel, F.: Journal of Computational Physics, 179 (2002), 1-6.
[2] Bosch, G. and Rodi, W.: International Journal for Numerical Methods in Fluids, 28 (1998), No. 4, 601-616.
[3] Rodi, W.: JSME International Journal Series B-Fluids & Thermal Engineering, 41 (1998), No. 2, 361-374.
[4] Rodi, W., et al.: Transactions of the ASME, 119 (1997), 248-262.
[5] Najjar, F.M., Thomas, B.G. and Hershey, D.E.: Metall. Trans. B, 26B (1995), No. 4, 749-765.
[6] Najjar, F.: Finite Element Modeling of Turbulent Fluid Flow and Heat Transfer Through Bifurcated Nozzles in Continuous Steel Slab Casters, University of Illinois at Urbana-Champaign, 1990, (M.S. Thesis).
[7] Hershey, D.E., Thomas, B.G. and Najjar, F.M.: Int. J. Num. Meth. in Fluids, 17 (1993), 23-47.
[8] Thomas, B.G., et al.: ISIJ International, 41 (2001), No. 10, 1262-1271.
[9] Thomas, B.G., O'Malley, R.J. and Stone, D.T.: "Measurement of temperature, solidification, and microstructure in a continuous cast thin slab", in: Modeling of Casting, Welding, and Advanced Solidification Processes, 1998, San Diego, CA: TMS, Warrendale, PA.
[10] Yuan, Q., Thomas, B.G. and Vanka, S.P.: Metallurgical and Materials Transactions B ,(2004), in press.
[11] Yuan, Q., Thomas, B.G. and Vanka, S.P.: Metallurgical and Materials Trans. B, (2004), in press.
[12] Horiuti, K.: Journal of the Physical Society of Japan, 54 (1985), No. 8, 2855-2865.
[13] CFX4.2. 1998, AEA Technology, 1700 N. Highland Rd., Suite 400, Pittsburgh, PA 15241.
[14] Creech, D.: Computational Modeling of Multiphase Turbulent Fluid Flow and Heat Transfer in the Continuous Slab Casting Mold, University of Illinois at Urbana-Champaign, 1998, (M.S. Thesis).
[15] Thomas, B.G. and Najjar, F.M.: Applied Mathematical Modeling, 15 (1991), 226-243.
[16] Harlow, F.H. and Welch, J.E.: Physics of Fluids, 8 (1965), No. 112, 2182-2189.
[17] Crank, J. and Nicolson, P.: Proc. Cambridge Philos. Soc., 43 (1947), 50-67.
[18] Sampine, L.F. and Gordon, M.K.: Computer Solution of Ordinary Differential Equations: the Initial Value Problem, 1975, San Francisco, W. H. Freeman & Company.
[19] User's Manual: Hypre - High Performance Preconditioners, 2001, Center for Applied Scientific Computing, Lawrence Livermore National Laboratory. p. 52.
[20] Winkler, C.M.: Large Eddy Simulations of Particle Dispersion and Deposition in a Turbulent Square Duct Flow, University of Illinois at Urbana-Champaign, 2002, (Dissertation).
[21] Zhao, B.: Numerical Study of Heat Transfer in Continuous Casting of Steel, University of Illinois at Urbana-Champaign, 2003, (M.S. Thesis).
[22] Yuan, Q., et al.: Metal. & Material Trans. B, in press (2004).
[23] Kubota, J., et al.: "Meniscus Flow Control in the Mold by Travelling Magnetic Field for High Speed Slab Caster", in: Steelmaking Conference Proceedings, 1991, Iron and Steel Society, Warrendale, PA. p. 233-241.
[24] Suzuki, M., et al.: "Flow Control of Molten Steel in Continuous casting Mold Using Travelling Magnetic Field", in: International Symposium on Electromagnetic Processing of Materials, 1994, ISIJ, Nagoya, Japan. p. 283-288.
[25] Huang, X., Thomas, B.G. and Najjar, F.M.: Metall. Trans. B, 23B (1992), No. 6, 339-356.
[26] Meng, Y. and Thomas, B.G.: Metallurgical and Materials Transactions B, 34B (2003), No. 5, 685-705.
[27] Jayatilleke, C.L.V.: "The Influence of Prandtl Number and Surface Roughness on the Resis-tance of the Laminar Sub-layer to Momentumand Heat Transfer", in: Progress in Heat and Mass Transfer, 1969, Pergamon Press Inc., p. 193-329.
[28] T. J. Craft, Graham, L.J.W. and Launder, B.E.: Int. J. Heat Mass Transfer, 36 (1993), No. 10, 2685-2697.
[29] Shi, T.: Effect of argon injection on fluid flow and heat transfer in the continuous slab casting mold, University of Illinois, 2001, (MS).
[30] Thomas, B.G., et al.: "Flow Dynamics and Inclusion Transport in Continuous Casting of Steel", in: 2004 NSF Design, Service, and Manufacturing Grantees and Research Conf. Proceedings. 2004, Southern Methodist University, Dallas, TX: Dallas, TX. p. 41.
[31] B. R. Hollworth and Gero, L.R.: Journal of Heat Transfer, 107 (1985), 910-915.